Self-Assembled Si(111) Surface States: 2D Dirac Material for THz Plasmonics

Z. F. Wang[1,2] and Feng Liu[2,3,*]
[1]Hefei National Laboratory for Physical Sciences at the Microscale, University of Science and Technology of China, Hefei, Anhui 230026, China
[2]Department of Materials Science and Engineering, University of Utah, Salt Lake City, Utah 84112, USA
[3]Collaborative Innovation Center of Quantum Matter, Beijing 100084, China
(Received 13 April 2015; published 7 July 2015)

Graphene, the first discovered 2D Dirac material, has had a profound impact on science and technology. In the last decade, we have witnessed huge advances in graphene related fundamental and applied research. Here, based on first-principles calculations, we propose a new 2D Dirac band on the Si(111) surface with $1/3$ monolayer halogen coverage. The sp^3 dangling bonds form a honeycomb superstructure on the Si(111) surface that results in an anisotropic Dirac band with a group velocity ($\sim 10^6$ m/s) comparable to that in graphene. Most remarkably, the Si-based surface Dirac band can be used to excite a tunable THz plasmon through electron-hole doping. Our results demonstrate a new way to design Dirac states on a traditional semiconductor surface, so as to make them directly compatible with Si technology. We envision this new type of Dirac material to be generalized to other semiconductor surfaces with broad applications.

DOI: 10.1103/PhysRevLett.115.026803 PACS numbers: 73.61.-r, 73.20.-r, 73.21.-b, 77.55.df

The semiconductor industry has been able to improve the performance of Si-based electronic devices by making them smaller and smaller, leading to denser, faster, and more power-efficient circuitry. However, this scaling and performance enhancement is not expected to continue forever, as it will encounter formidable scientific and technical challenges. Therefore, it is becoming urgent to develop alternative device technologies. Besides the development of new operating principles, for example, spin- and valley-based devices [1,2], another approach is to replace the conducting channels in Si-based devices with low-dimensional materials, which have superior electrical properties. In this regard, the emergence of 2D membrane materials [3–5] such as graphene, layered metal dichalcogenides, and semiconductor nanomembranes [6–8] opens a new avenue for next-generation nanoelectronic devices, especially affording a novel 2D platform for highly foldable and adaptable device components.

Because of the extraordinary properties of the linear Dirac band in graphene [9], a host of applications have been proposed, including electronics, biological engineering, photovoltaics, and energy storage [10]. To go beyond graphene, researchers have tried to realize graphenelike material in other systems, such as the new material category called 2D Dirac materials [11,12]. These 2D Dirac materials also offer a tunable platform to study topological and correlated phases [13–18]. So far, several experimental methods have been reported to realize the artificial Dirac materials, including nanopatterning of 2D electron gases [19], molecular assembling by scanning probe microscopy [20], and optical trapping of ultracold atoms [21]. Despite the tremendous promise offered by the 2D Dirac materials, a foreseeable challenge is to integrate them with the existing Si technology, but without being bound by the planar geometry of the existing platform of solid substrates.

To gain the merits of both Si technology and Dirac states, the best way is to combine them and design Si-based Dirac materials. Silicene, the 2D monolayer Si with a honeycomb structure, has been proposed under this background. Recently, silicene has been grown on Ag, ZrB_2, and Ir substrates [22–24], but the strong hybridization between silicene and the substrate significantly deteriorates its electronic properties [25]. Chen *et al.* found a Dirac-like surface state in a Si(111) thin film grown on a Ag(111) substrate [26] that has a $\sqrt{3} \times \sqrt{3}R30°$ honeycomb superstructure. The Dirac band dispersion in their work is obtained from the quasiparticle interference patterns on the surface. However, due to the limited data points around small momentum regions, such an indirect classification method has been questioned [27]. Until now, there is no direct evidence to confirm the realization of the Dirac state in Si materials.

In this Letter, based on first-principles calculations, we propose a chemical engineering method to create a 2D Dirac state on the Si(111) surface. Halogen atoms prefer to saturate the Si(111) surface dangling bonds and distribute uniformly on the surface due to Coulomb and steric repulsion. At $1/3$ monolayer (ML) halogen coverage, a $\sqrt{3} \times \sqrt{3}R30°$ honeycomb superstructure is formed, and the unsaturated sp^3 dangling bonds will generate an anisotropic Dirac band. Most remarkable, under electron-hole doping, the Si-based surface Dirac band can be used to excite a tunable THz plasmon. Considering the experimental feasibility, we believe this new type of Dirac material will have a great chance of being confirmed in the near future.

 © 2015 American Physical Society

The first-principles calculations are carried out in the framework of the generalized gradient approximation with Perdew-Burke-Ernzerhof (PBE) and Heyd-Scuseria-Ernzerhof (HSE) functionals using the Vienna *ab initio* simulation package (VASP) [28]. The $\sqrt{3}\times\sqrt{3}R30°$ $[3\sqrt{3}\times 3\sqrt{3}R30°]$ Si(111) surface is simulated by 12-layer [four-layer] Si slabs, and the bottom surface is saturated by hydrogen atoms. All the calculations are performed with a plane-wave cutoff of 500 eV on the $15\times 15\times 1$ Monkhorst-Pack k-point mesh. The vacuum layer is 15 Å thick to ensure decoupling between neighboring slabs. During structural relaxation, the halogen and top four-layer Si atoms are relaxed until the forces are smaller than 0.01 eV/Å. Without losing generality, in the present work we will focus on the Br atom as a typical halogen atom.

First, we discuss the experimental feasibility of obtaining our proposed Br adsorbed Si(111) superstructure. As the basic material used in the semiconductor industry, the surface of Si has been extensively studied. At low temperatures, the Si(111) surface has a complex (7×7) reconstructed structure [29], because the reconstruction can eliminate the dangling bonds and reduce the surface energy. However, at high temperatures, the Si(111) surface can retain an unreconstructed (1×1) structure with one dangling bond on each surface atom [30]. In addition, the hydrogenated Si(111) surface also retains the 1×1 structure [30]. Thirty years ago, x-ray standing-wave experiments actually showed that Br atoms prefer to be chemisorbed at the top position (above a Si atom) of the unreconstructed Si(111) surface, and to form a $\sqrt{3}\times\sqrt{3}R30°$ honeycomb superstructure at 1/3 ML Br coverage [31,32].

Next, we discuss the theoretical rational for the above experimental results. We have compared the binding energy for different Br adsorption sites on the Si(111) surface. The binding energy is in descending order −3.88, −2.54, and −2.37 eV from the top (T), to the H, to the $T4$ positions, as shown in Fig. 1(a). To check the stable pattern of 1/3 ML Br coverage on the Si(111) surface, we have chosen a large $3\sqrt{3}\times 3\sqrt{3}R30°$ supercell, and adsorbed nine Br atoms in the surface. As shown in Fig. 1, Br atoms prefer a uniform distribution at 1/3 ML coverage, resulting in a $\sqrt{3}\times\sqrt{3}R30°$ superstructure [Fig. 1(a)], and its energy is much lower than that of a random [Figs. 1(b) and 1(c)] or a cluster [Figs. 1(d) and 1(e)] distribution. We also checked that the preferred stable uniform distribution is not affected by either n- or p-type doping. In addition, the proposed structure is kinetically stable, with a sizable energy barrier of ∼1.1 eV for Br to diffuse out of the T site. To get a better understanding of this phenomenon, we analyze the interaction between Br and the Si(111) surface. Based on Bader charge analysis, we found that there are 0.2 electrons transferred from Si to Br. Therefore, due to the Coulomb repulsion, the negatively charged Br atoms will have a steric repulsion to each other, resulting in a uniform

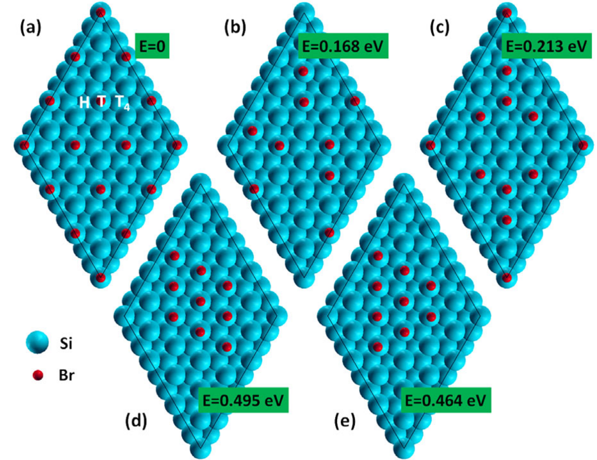

FIG. 1 (color online). (a)–(e) Energy comparison for different Br adsorption configurations on a Si(111) surface at 1/3 ML coverage in a $3\sqrt{3}\times 3\sqrt{3}R30°$ supercell. The Br atoms are distributed uniformly in configuration (a), randomly in configurations (b) and (c), and form clusters in configurations (d) and (e). The energy for configuration (a) is set as the reference energy. The labels T, H, and $T4$, shown in (a), denote different adsorption positions for the Br atom.

distribution. Although the x-ray measurement did not directly show the Si superstructure at 1/3 Br ML coverage [31,32] (no scanning tunneling microscope or angle-resolved photoemission spectroscopy at that time), the good agreement between our theoretical calculations and the x-ray experiments nevertheless strongly supports the existence of the proposed Si superstructure.

In the following, we turn to the focus of this work, the electronic structures of the proposed Br adsorbed Si superstructure. As a comparison, the bare $\sqrt{3}\times\sqrt{3}R30°$ Si(111) surface without Br adsorption is studied first. The most important finding is that there is a Dirac cone at the K point around the Fermi level in the band gap region, as shown in Fig. 2(a). This may explain why a Dirac-like surface state is observed in Chen *et al.*'s experiment [26]. However, an extra band is also found in the same energy window. Thus, the band in Fig. 2(a) is not a real Dirac band, because the extra band will mitigate the Dirac band properties. The origin of all three bands can be easily understood. They are the surface bands and come from the three dangling bonds in the unit cell. One straightforward way to eliminate the extra band is to saturate one dangling bond [16], leaving only two dangling bonds in the unit cell. This is the reason why we choose the 1/3 ML Br adsorbed Si(111) surface, whose band structure is shown in Fig. 2(b). We can see that only two surface bands are left, forming a Si-based surface Dirac band. The orbital projected density of states (PDOS) of the Dirac band is shown in Fig. 2(c). One s and three p orbits have contributions to the Dirac band, demonstrating an sp^3 hybridization feature. In these four orbits, p_z has the largest contribution, while s, p_x, and

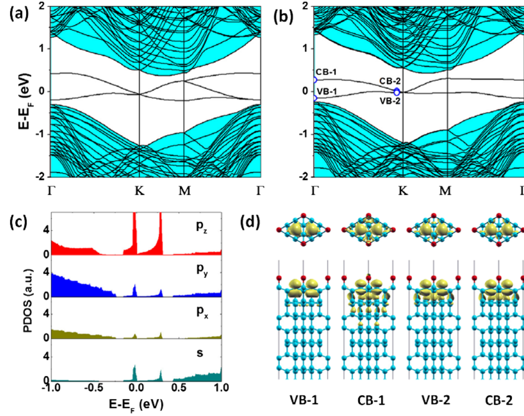

FIG. 2 (color online). (a),(b) Band structures of the $\sqrt{3}\times\sqrt{3}R30°$ Si(111) surface without and with Br adsorption. The shadow regions are the bulk states. (c) Projected density of states of the Dirac band shown in (b), showing the different orbital components. (d) Top and side view of the partial charge density of the Dirac band at the four chosen k points labeled in (b). For clarity, only the top part of the substrate is plotted in the side view.

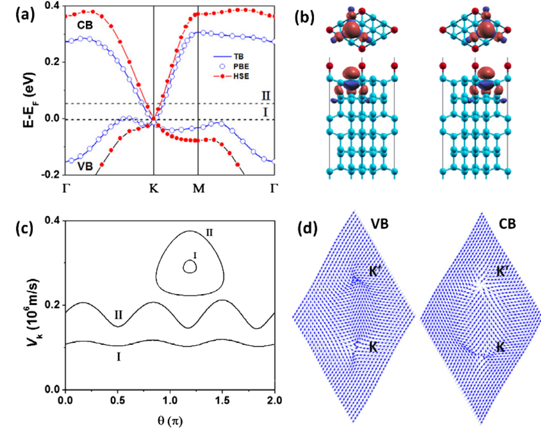

FIG. 3 (color online). (a) Enlargement of Dirac band structures obtained from TB, and first-principles with PBE and HSE functionals. (b) Top and side view of two MLWFs fitted from the PBE Dirac band. The red and blue colors denote positive and negative values, respectively. (c) The component of the group velocity parallel to the $\mathbf{k}$ vector [$V_k = \mathbf{V}(\mathbf{k})\cdot\hat{k}$ with $\mathbf{k}$ measured from the Dirac point] for the Dirac band at energy I and II marked by the dashed lines in (a). The insets are the isosurfaces of the Dirac band at energy I and II. (d) Pseudospin textures of VB and CB Dirac bands.

p_y have a similar contribution. To illustrate the surface nature of this Dirac band, four k points [two for both the valence band (VB) and the conduction band (CB)] are chosen at Γ and near K, as labeled in Fig. 2(b). The corresponding partial charge densities are shown in Fig. 2(d), which are localized around two surface dangling bonds and are characterized by an sp^3 orbital shape.

Since the Si-based surface Dirac band is separated from the bulk bands and is completely isolated in the band gap region, we can write an effective tight-binding (TB) Hamiltonian to describe it. By using the maximally localized Wannier functions (MLWFs) in the WANNIER90 package [33], a 2×2 effective Hamiltonian is constructed. As shown in Fig. 3(a), the TB band shows good agreement with the PBE first-principles band. The two fitted MLWFs are shown in Fig. 3(b), in which we can clearly see the sp^3 nature of the Dirac band. To further support our results, the Dirac band obtained from the first-principles calculations with the HSE functional is also plotted in Fig. 3(a). For the HSE Dirac band, the splitting between the VB and CB becomes larger. Meanwhile, the Dirac point is no longer buried by the VB band anymore. Overall, this feature of the Dirac band is not changed by using different functionals, demonstrating the reliability of our results. For the Si-based surface Dirac band shown in Fig. 3(a), its band width (∼0.5 eV) is very narrow and its electron or hole symmetry is broken even in the low energy region.

The group velocity is one of the key parameters in the study of Dirac materials, as it bears a variety of fundamental information [34]. Here, we focus on the CB band, since the VB band is skewed from the linear dispersion. At two given energies, marked by the dashed lines (I and II) in Fig. 3(a), the group velocities (V_k) and isosurfaces of the Dirac band are shown in Fig. 3(c). Two features are noticeable. First, the group velocity is anisotropic and oscillates with a period of $2\pi/3$. Second, the amplitude of the oscillation increases with energy going away from the Dirac point. Therefore, the Si-based surface Dirac band is a highly reshaped anisotropic Dirac band, which calls for further study in terms of Dirac band physics. The pseudospin is another key parameter for the Dirac band, as the physical origin for many interesting phenomena [9]. The pseudospin textures of the VB and CB are shown in Fig. 3(d). Around two inequivalent Dirac points (K and K'), the pseudospin has a vortex and antivortex texture, and these textures are inverse with each other for the VB and CB. In addition, the pseudospin has only in-plane components. Thus, the topological number will be zero for both the VB and CB. If a nontrivial gap is opened at the Dirac point by either spin-orbital coupling or inversion symmetry breaking, different topological phases can be studied [2,13–16].

As an potential application of our proposed Si-based surface Dirac band, its collective plasmon excitation is also calculated. Using the Lindhard function [35], the non-interacting polarization function $\Pi(\mathbf{q},\omega)$ can be written as

$$\Pi(\mathbf{q},\omega) = -\frac{2}{(2\pi)^2}\int_{\mathrm{BZ}} d^2\mathbf{k}\sum_{l,l'}|\langle\mathbf{k}+\mathbf{q},l'|e^{i\mathbf{q}\cdot\mathbf{r}}|\mathbf{k},l\rangle|^2 \times\frac{f(E_{\mathbf{k},l})-f(E_{\mathbf{k}+\mathbf{q},l'})}{E_{\mathbf{k},l}-E_{\mathbf{k}+\mathbf{q},l'}+\omega+i\delta}, \quad (1)$$

where the integral is over the first Brillouin zone (BZ). A temperature $T = 300$ K in the Fermi-Dirac distribution function and an infinitesimal broadening $\delta = 1$ meV are

used in our numerical calculation. Under the random phase approximation, the dielectric function is defined as

$$\varepsilon(\mathbf{q}, \omega) = 1 - V(\mathbf{q})\Pi(\mathbf{q}, \omega), \tag{2}$$

where $V(\mathbf{q}) = 2\pi e^2/4\pi\epsilon_0\epsilon_r q$ is the Fourier component of the 2D Coulomb interaction. ϵ_0 and ϵ_r are the vacuum and background relative dielectric constants, respectively, and we set $\epsilon_r = 11$ for the Si. The collective plasmon excitation mode is defined at zeros of the dielectric function. In general, the dielectric function is complex. Therefore, the complex solution at $\varepsilon = 0$ gives both the plasmon dispersion (real part) and the decay of the plasmon (imaginary part). In order to compare with the experiments, it is more convenient to calculate the electron energy loss spectrum (EELS), whose broadened peaks indicate the plasmons,

$$\mathrm{EELS} = -\mathrm{Im}[1/\varepsilon(\mathbf{q}, \omega)]. \tag{3}$$

The EELS of the Si-based surface Dirac band is shown in Fig. 4, from which we can seen how the plasmon dispersion changes with the Fermi level. For hole doping ($E_F = -0.1$ eV), the plasmon dispersion has a wide distribution in the window of energy and momentum space, but its shape is a little different along the q_x and q_y directions, as shown in Figs. 4(a) and 4(b), respectively. To clearly illustrate this anisotropy, the EELS in 2D momentum space at four excitation energies is shown in Fig. 4(c). We can see that the plasmon dispersion is an ellipse at each energy, and the anisotropy becomes larger for higher energy. In the small momentum region, the plasmon is

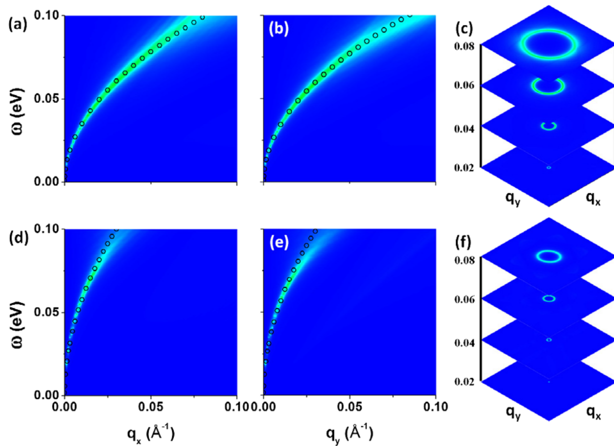

FIG. 4 (color online). EELS of the hole (a),(b),(c) and electron (d),(e),(f) doped Dirac band with $E_F = -0.1$ and 0.1 eV, respectively. (a) and (d) are excitations along the q_x direction with $q_y = 0$. (b) and (e) are excitations along the q_y direction with $q_x = 0$. (c) and (f) are 2D momentum space plots of the EELS at different excitation energies. The open black circles are fitted using $\omega = \alpha\sqrt{q}$ with $\alpha = 0.35$, 0.345, 0.575, and 0.57 eV/Å$^{-1/2}$ for (a), (b), (d), and (e), respectively.

dominated by the intraband transition, and it is not damped. But in the large momentum region, the plasmon will undergo an interband transition, become damped, and decay into electron or hole pairs. This is consistent with the gradually increased plasmon peak width with increasing momentum, as shown in Figs. 4(a)–4(c).

For the Dirac band in graphene, its plasmon follows the rule of $\omega \propto \sqrt{q}$ in the small momentum region [36]. For the Si-based surface Dirac band, despite the anisotropic shape, we found that its plasmon can still be qualitatively described by the same rule, as shown by the fitting of the open black circles in Figs. 4(a) and 4(b). For electron doping ($E_F = 0.1$ eV), similar anisotropy and scaling behavior have been observed. However, the slope of the plasmon is larger than that in hole doping, and the plasmon has a narrow distribution in the window of energy and momentum space, as shown in Figs. 4(d)–4(f). Therefore, for the same excitation momentum, the plasmon will have a higher energy in the case of electron doping than that in hole doping, indicating an effective way to manipulate the plasmon dispersion through doping. Since our designed Dirac band is on the Si surface and its band width is very narrow, it is more convenient to tune its Fermi level through the electric gating method. The carrier density needed for shifting the Fermi level by 0.1 eV (-0.1 eV) is about $\sim 6 \times 10^{13}$ cm^{-2} (4×10^{14} cm^{-2}). This is a rather typical doping level for 2D Dirac materials like graphene, which is readily accessible by either gating or chemical doping as shown by previous experiments [37,38]. Usually, the bulk Si doping level is in the range of 10^{13}–10^{20} cm^{-3}, which would translate to a 2D density of 10^{7}–10^{14} cm^{-2} assuming even a small layer thickness of 10 nm. In addition, special doping methods such as δ doping might be used to enhance locally 2D doping.

Our designed Si-based surface Dirac band comes from the surface dangling bonds, so it may not be stable under ambient conditions. In order to protect the Dirac band, the best way is to put a chemically inert layer on top of it. Here, we will use the monolayer BN, because of its chemical inactivity, large band gap, and small lattice mismatch to Si(111) (∼0.1%). Using the van der Waals–density functional theory method, the optimized structure for BN on Br adsorbed Si substrate is shown in Fig. 5(a). The vertical distance between BN and Br is 3.17 Å, indicating a weak

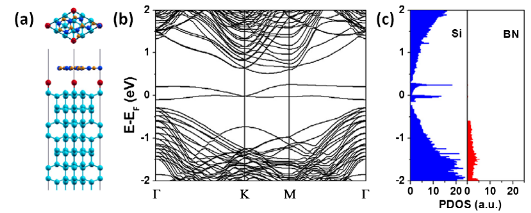

FIG. 5 (color online). (a), (b), and (c) are the atomic structure, band structure, and projected density of states for a BN protected Si(111) surface with 1/3 ML Br coverage.

interaction between them. The band structure of Br adsorbed Si with a BN protective layer is shown in Fig. 5(b). Comparing with the case without BN [Fig. 2(b)], the Dirac band is almost unchanged. The corresponding PDOS is shown in Fig. 5(b), confirming that no BN band overlaps with the Dirac band. Therefore, the Si-based surface Dirac band can be made very robust by including a BN protective layer.

In conclusion, we demonstrate a novel form of 2D Dirac materials, which are created on the Si(111) surface by the self-assembled surface adsorption of Br atoms. While much recent attention has been paid to freestanding 2D materials, we believe our approach offers an important alternative in substrate-supported 2D materials whose electronic bands are completely isolated from the underlying substrate bands, so that they behave electronically just like freestanding 2D materials but are structurally stable. Furthermore, our finding may ease the way for future applications of 2D materials by its inherent compatibility with current semiconductor technology.

Z. F. W. acknowledges support from NSF-MRSEC (Grant No. DMR-1121252), F. L. acknowledges support from U.S. DOE-BES (Grant No. DE-FG02-04ER46148). We thank NERSC and CHPC at the University of Utah for providing the computing resources.

[*]fliu@eng.utah.edu

[1] P. Avouris, Z. Chen, and V. Perebeinos, Nat. Nanotechnol. **2**, 605 (2007).
[2] X. Xu, W. Yao, D. Xiao, and T. F. Heinz, Nat. Phys. **10**, 343 (2014).
[3] S. Z. Butler *et al.*, ACS Nano **7**, 2898 (2013).
[4] G. Fiori, F. Bonaccorso, G. Iannaccone, T. Palacios, D. Neumaier, A. Seabaugh, S. K. Banerjee, and L. Colombo, Nat. Nanotechnol. **9**, 768 (2014).
[5] P. Miro, M. Audiffred, and T. Heine, Chem. Soc. Rev. **43**, 6537 (2014).
[6] F. Liu and M. G. Lagally, Chem. Rev. **97**, 1045 (1997).
[7] J. Zang, M. Huang, and F. Liu, Phys. Rev. Lett. **98**, 146102 (2007).
[8] M. Huang, C. Boone, M. Roberts, D. E. Savage, M. G. Lagally, N. Shaji, H. Qin, R. Blick, J. A. Nairn, and F. Liu, Adv. Mater. **17**, 2860 (2005).
[9] A. H. Castro Neto, F. Guinea, N. M. R. Peres, K. S. Novoselov, and A. K. Geim, Rev. Mod. Phys. **81**, 109 (2009).
[10] K. S. Novoselov, V. I. Fal′ko, L. Colombo, P. R. Gellert, M. G. Schwab, and K. Kim, Nature (London) **490**, 192 (2012).
[11] T. O. Wehling, A. M. Black-Schaffer, and A. V. Balatsky, Adv. Phys. **63**, 1 (2014).
[12] M. Polini, F. Guinea, M. Lewenstein, H. C. Manoharan, and V. Pellegrini, Nat. Nanotechnol. **8**, 625 (2013).
[13] Z. F. Wang, Z. Liu, and F. Liu, Nat. Commun. **4**, 1471 (2013).
[14] L. Miao *et al.*, Proc. Natl. Acad. Sci. U.S.A. **110**, 2758 (2013).
[15] Z. F. Wang, Z. Liu, and F. Liu, Phys. Rev. Lett. **110**, 196801 (2013).
[16] M. Zhou, W. Ming, Z. Liu, Z. F. Wang, P. Li, and F. Liu, Proc. Natl. Acad. Sci. U.S.A. **111**, 14378 (2014).
[17] M. S. Miao, Q. Yan, C. G. Van de Walle, W. K. Lou, L. L. Li, and K. Chang, Phys. Rev. Lett. **109**, 186803 (2012).
[18] D. Zhang, W. Lou, M. Miao, S.-C. Zhang, and K. Chang, Phys. Rev. Lett. **111**, 156402 (2013).
[19] A. Singha *et al.*, Science **332**, 1176 (2011).
[20] K. K. Gomes, W. Mar, W. Ko, F. Guinea, and H. C. Manoharan, Nature (London) **483**, 306 (2012).
[21] L. Tarruell, D. Greif, T. Uehlinger, G. Jotzu, and T. Esslinger, Nature (London) **483**, 302 (2012).
[22] P. Vogt, P. De Padova, C. Quaresima, J. Avila, E. Frantzeskakis, M. C. Asensio, A. Resta, B. Ealet, and G. Le Lay, Phys. Rev. Lett. **108**, 155501 (2012).
[23] A. Fleurence, R. Friedlein, T. Ozaki, H. Kawai, Y. Wang, and Y. Yamada-Takamura, Phys. Rev. Lett. **108**, 245501 (2012).
[24] L. Meng *et al.*, Nano Lett. **13**, 685 (2013).
[25] Y.-P. Wang and H.-P. Cheng, Phys. Rev. B **87**, 245430 (2013).
[26] J. Chen, W. Li, B. Feng, P. Cheng, J. Qiu, L. Chen, and K. Wu, arXiv:1405.7534.
[27] R. Arafune, C.-L. Lin, R. Nagao, M. Kawai, and N. Takagi, Phys. Rev. Lett. **110**, 229701 (2013).
[28] G. Kresse and J. Hafner, Phys. Rev. B **47**, 558 (1993).
[29] J. G. Hou, J. Yang, H. Wang, Q. Li, C. Zeng, H. Lin, W. Bing, D. M. Chen, and Q. Zhu, Phys. Rev. Lett. **83**, 3001 (1999).
[30] F. Liu, M. Hohage, and M. G. Lagally, *Encyclopedia of Applied Physics* (Wiley-VCH Verlag GmbH, London, 1999), p. 321.
[31] B. N. Dev, V. Aristov, N. Hertel, T. Thundat, and W. M. Gibson, Surf. Sci. **163**, 457 (1985).
[32] H.-S. Cheng, L. Luo, M. Okamoto, T. Thundat, S. Hashimoto, and W. M. Gibson, J. Vac. Sci. Technol. A **5**, 607 (1987).
[33] A. A. Mostofi, J. R. Yates, Y.-S. Lee, I. Souza, D. Vanderbilt, and N. Marzari, Comput. Phys. Commun. **178**, 685 (2008).
[34] Z. F. Wang, L. Chen, and F. Liu, Nano Lett. **14**, 2879 (2014).
[35] K. W.-K. Shung, Phys. Rev. B **34**, 979 (1986).
[36] E. H. Hwang and S. Das Sarma, Phys. Rev. B **75**, 205418 (2007).
[37] D. K. Efetov and P. Kim, Phys. Rev. Lett. **105**, 256805 (2010).
[38] Y. Kim, J. Ryu, M. Park, E. S. Kim, J. M. Yoo, J. Park, J. H. Kang, and B. H. Hong, ACS Nano **8**, 868 (2014).